Materials Science & Engineering A 756 (2019) 156–160

Contents lists available at ScienceDirect

Materials Science & Engineering A

journal homepage: www.elsevier.com/locate/msea

Short communication

Modelling strengthening mechanisms in beta-type Ti alloys

G.-H. Zhao, X.Z. Liang, B. Kim, P.E.J. Rivera-Díaz-del-Castillo*

Department of Engineering, Lancaster University, Lancaster, LA1 4YK, UK

ARTICLE INFO

Keywords:
Ti alloys
Plasticity modelling
Strengthening mechanisms
Dislocation theory

ABSTRACT

An integral modelling approach for understanding the strengthening mechanisms in Ti alloys is presented and applied to alloys undergoing deformation via dislocation slip. The model incorporates contributions from solid solution, grain boundary, dislocation forest and strain hardening. The metal forming and thermomechanical processing factors influence both grain size and the stored strain energy. The strain hardening of Ti-Fe-Sn-Nb alloys was modelled by considering dislocation accumulation and annihilation terms. By tailoring the contribution of each strengthening effect, the yield stress and plasticity of advanced Ti alloys can be optimised.

1. Introduction

β-type titanium alloys with a bcc lattice have been applied as engineering materials, attracting a great deal of attention owing to a combination of high specific strength, good ductility and a relatively low elastic modulus. They exhibit flexible mechanical properties and β-stability-sensitive deformation mechanisms which result from a trade between dislocation slip, mechanical twinning and stress-induced phase transformation. Similar to steels, the composition-dependent activation energy for dislocation slip may be higher than that of twinning and martensite formation [1]. Thus, the slip-dominated Ti alloys are known to exhibit the highest yield strength. The dislocation slip in β-Ti alloys, like other bcc metals, mainly occurs with $a/2\langle 111\rangle$ Burgers vectors, gliding on {110}, {112} or {123} planes [2]. The critical resolved shear stress (CRSS) to activate slip is an important factor for mechanical calculations, and determines the macroscopic yield stress. It is therefore crucial to quantitatively understand the contributions from each strengthening mechanism. In this letter, we aim at building an integral approach to quantify the strength of β-Ti alloys by incorporating the influence from solid-solution hardening, grain boundary strengthening, as well as forest and strain hardening. The proposed modelling approach provides a guideline for optimising alloys with a good combination of strength and plasticity.

2. Modelling

Solid-solution hardening (SSH) results from the interaction between dislocations and solute atoms, where dislocation movements are impeded by such interaction. In binary systems, the CRSS, τ_{CRSS}, to move a dislocation through a random array of obstacles satisfies the following equation [3,4]:

$$\tau_{CRSS} = \tau_0 + \mu\lambda^{4/3}X_i^{2/3}Z \quad (1)$$

where τ_0 is the CRSS of the pure Ti, μ is the shear modulus of the alloy and X_i is the concentration of solute i (at.%). λ is a misfit parameter accounting for the solute/solvent lattice parameter misfit (δ) and the shear modulus misfit (η) between Ti and the foreign atoms. Z is a temperature-dependent numerical factor whose value can be obtained from a plot of $(d\tau/dX_i^{2/3})$ versus $\lambda^{4/3}$ by Eq. (1). $Z = 0.9 \times 10^{-3}$ [4] is adopted in current work. The formulation was further extended to multicomponent systems by Gypen [5] and Toda-Caraballo [6], expressing the normal stress generated by SSH as:

$$\sigma_{ss} = \left(\sum_i B_i^{3/2}X_i\right)^{2/3};\ B_i = M\mu\lambda_i^{4/3}Z \quad (2)$$

where M is the Taylor factor, an average orientation factor that depends on the texture of the material and on the crystallographic nature of the assumed slip systems. $M = 2.8$ was calculated as the average value of mixed $\{110,112,123\}\langle 111\rangle$ slip for bcc metals [7]. B_i represents the strengthening coefficient of SSH for solute i, which accounts for the alloy shear modulus and the misfit parameter λ expressed as [6]:

$$\lambda_i = \xi(\eta_i'^2 + \theta^2\delta_i^2)^{1/2} \quad (3)$$

where $\eta'_i = \frac{\eta_i}{1+0.5\,|\,\eta_i|}$; $\xi = 1$ for fcc metals while $\xi = 4$ for bcc metals [6]. θ describes the difference in the interaction forces between screw and edge dislocations, it is generally accepted that $3 < \theta < 16$ for screw dislocations and $\theta > 16$ for edge dislocations [4]. The shear modulus misfit η_i and lattice parameter misfit δ_i are respectively expressed as [6]:

* Corresponding author.
E-mail address: p.rivera1@lancaster.ac.uk (P.E.J. Rivera-Díaz-del-Castillo).

https://doi.org/10.1016/j.msea.2019.04.027
Received 4 February 2019; Received in revised form 3 April 2019; Accepted 5 April 2019
Available online 11 April 2019

$$\eta_i = \frac{d\mu_i}{dX_i}\frac{1}{\mu_{Ti}}; \quad \delta_i = \frac{da_i}{dX_i}\frac{1}{a_{Ti}} \tag{4}$$

where a is the lattice parameter and η_i can be approximated by $\eta_i = \frac{2(\mu_i - \mu_{Ti})}{\mu_i + \mu_{Ti}}$ [6].

The Hall-Petch relation is applied to calculate the grain boundary strengthening, which describes an inverse dependence between the yield stress and the mean grain size D:

$$\sigma_{HP} = \sigma_0 + \frac{k_Y}{\sqrt{D}} \tag{5}$$

where σ_0 refers to the friction stress, and k_Y is the Hall-Petch constant. The dependence of k_Y on shear modulus μ and the magnitude of the Burgers vector b is considered in different models [8]. An expression for k_Y was derived as $k_Y = k_{Ti} + \sum_i k_i X_i$ [8] where $k_{Ti} = 0.75\,\mathrm{MPa{\cdot}m^{1/2}}$ for pure Ti. The values of k_i for alloying elements are adopted from Ref. [9].

The forest strengthening originates from dislocation interactions. When two dislocations glide on different slip planes crossing each other, their total energy can be reduced by reacting to form a third junction dislocation segment [10]. The forest strengthening describes the shear stress τ to destroy a junction barrier and remobilize the dislocation line with the relationship $\tau \propto \mu b/l$, where l is the distance between the intersecting obstacles along the dislocation line. The average value of the distance scales as $1/\sqrt{\rho}$, where ρ is the dislocation density. This leads to a well-known relationship to calculate the forest hardening $\sigma_\rho = \alpha\mu b M\sqrt{\rho}$ [11], where $\alpha = 0.3$ reflects the average strength of dislocation interactions (junction strength) over all existing configurations [12].

The strain hardening and the evolution of the flow stress are considered for the plastic deformation region. Whereas the storage is known to result in a linear and athermal deformation stage, dynamic recovery describes a temperature and strain rate-sensitive process, during which the strain hardening rate continuously decreases due to rearrangement and annihilation of dislocations [12]. This leads to the Kocks-Mecking equation expressing the competition between storage and annihilation terms [13]: $\frac{d\rho}{d\gamma} = \frac{1}{b\Lambda} - f\rho$. γ is the shear strain, Λ is the dislocation mean free path representing the distance travelled by a dislocation segment before it is stored by interaction with the microstructure [14]. f is a parameter describing the dislocation annihilation due to dynamic recovery.

Considering the grain boundaries and dislocation junctions as obstacles, $\frac{1}{\Lambda} = \frac{1}{D} + k\sqrt{\rho}$. where k is the dislocation storage coefficient. This leads to the evolution of dislocation density as a function of macroscopic strain:

$$\frac{d\rho}{d\varepsilon} = M\left[\frac{k}{b}\sqrt{\rho} + \frac{1}{bD} - f\rho\right] \tag{6}$$

For Ti alloys operating dislocation slip dominated deformation feature, an integral expression of their yield stress becomes:

$$\sigma_Y = \sigma_{Ti} + \alpha M\mu b\sqrt{\rho} + \left(\sum_i B_i^{3/2} X_i\right)^{2/3} + \frac{k_{Ti} + \sum_i k_i X_i}{\sqrt{D}} \tag{7}$$

by combining the critical slip-activation stress of pure Ti, σ_{Ti}, the contribution of solid solution hardening σ_{ss}, grain boundary hardening σ_{HP} and the forest dislocation hardening σ_ρ.

3. Materials and methods

We initially apply the model to a series of high-strength Ti alloys with nominal compositions of Ti-11Fe-7Sn-5Nb, Ti-13Fe-7Sn-5Nb and Ti-15Fe-7Sn-5Nb (wt.%). Fe was added as main alloying element, besides it is the strongest β-stabilizer as 3.5 wt.% Fe is sufficient to retain full β-phase during quenching [15]. A Ti-Fe binary phase diagram is calculated by Thermo-Calc using the database TCTI1: Ti-Alloys in

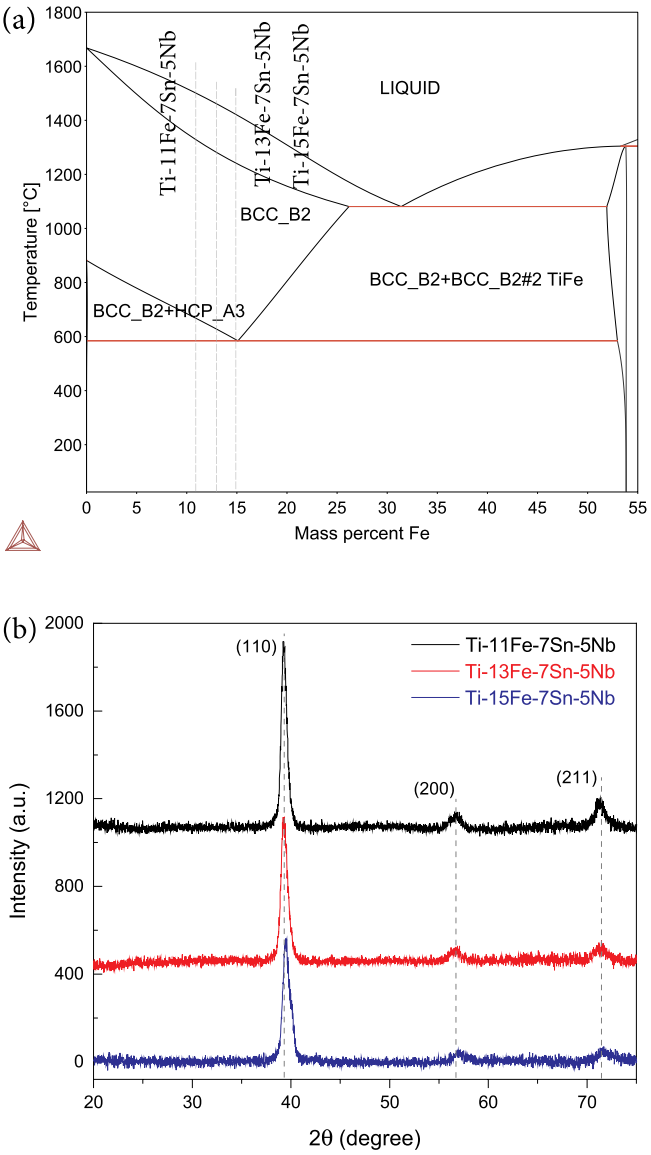

Fig. 1. (a) The Ti-Fe phase diagram calculated by Thermo-Calc using TCTI1:Ti-Alloys database. The compositions of the alloys were designed to be hypoeutectoid in order to avoid the formation of TiFe intermetallic phase; (b) XRD patterns of the as-cast Ti-Fe-Sn-Nb alloys showing full β-phase microstructure.

Fig. 1(a). The model alloys were prepared by arc-melting followed by injection casting. The samples are cylindrical with a diameter of 3 mm in order to achieve a rapid overall cooling rate of ($10^3 \sim 10^4$ K/s). The as-cast alloys showed a supersaturated single β-Ti phase in Fig. 1(b) with a mean grain size of 12 μm [16]. The operative deformation model is dislocation slip, no evidence of mechanical twinning or strain-induced phase transformation was observed due to the highly stabilized β-phase [17].

During rapid solidification, a considerable fraction of the deformation energy is stored in the form of elastic energy, which is due to the strain fields of the generated dislocations [18]. For an elastically isotropic material, Stibitz equation relates the stored volumetric energy W to the mean relative change in lattice spacing $\Delta d/d$ [18]:

$$W = \frac{3E}{2(1+2\nu^2)}\left(\frac{\Delta d}{d}\right)^2 \tag{8}$$

E and ν refers elastic modulus and Poisson's ratio, respectively. The relative change in lattice spacing can be obtained from the broadening

of Bragg peaks.

X-ray diffraction line profiles are analysed to evaluate the stored elastic energy. The overall broadening can be measured by the diffraction peak's full-width at half maximum (FWHM). However, one should keep in mind that broadening is often caused by crystal structure imperfections (crystallite size, microstrains or faulting), as well as by external factors (instrumental broadening). In order to isolate the effect of microstrain ε_{micro} induced by an increase in the dislocation density, Rietveld refinement was performed by MAUD software on the XRD patterns [19]. A Si single crystal standard was used to obtain the instrumental broadening information. The dislocation elastic energy w stored per unit length can be reasonably approximated by $w = \mu b^2/2$. The average dislocation density ρ can then be correlated to the microstrain [20]:

$$\rho = \frac{W}{w} = \frac{3E}{\mu b^2(1+2\nu^2)}\varepsilon_{micro}^2 \tag{9}$$

4. Results and discussion

In order to quantitatively evaluate the solid-solution hardening coefficient, Fig. 2 presents the shear modulus mismatch *vs*. the atomic radius mismatch of the solutes in Ti alloys. The values of shear moduli and atomic radii are shown in Table 1. Seitz radii R are used because they are related to the lattice parameter by $R = (3\phi/4\pi c)^{1/3}a$ [21], where c refers to the number of atoms per unit cell and ϕ is a constant that depends on the lattice structure.

The strengthening coefficients B_i in Eq. (2) were calculated for each alloying element (Table 1). The most significant SSH effect comes from Pd due to its larger atomic size difference with Ti. For similar reasons, Pd is known to be an effective glass-forming element in Ti-based bulk metallic glasses, as it induces topological instabilities that promote the formation of close-packed atomic clusters [22]. The large strengthening coefficients also come from eutectoid β-stabilizers such as Cr, Co, Ni, Fe and Cu, while isomorphous stabilizers such as Mo, Ta and Nb present limited or weak strengthening effects.

The strengthening mechanisms combining solid solution, grain boundary and dislocation forest hardening was applied to the Ti-Fe-Sn-Nb model alloys. For fcc and bcc metals with lattice parameter a, the magnitude of Burgers vector $b = (a/2)\sqrt{h^2+k^2+l^2}$. Considering the closest-packed crystallographic system for bcc metals is $\{110\}\langle 111\rangle$, the corresponding magnitude of b is determined by $(\sqrt{3}/2)a$. Although the lattice parameter slightly decreases with increasing solute concentration, we take the mean measured value $a = 3.325$ Å [17] and thus $b = 2.8$ Å for all calculations.

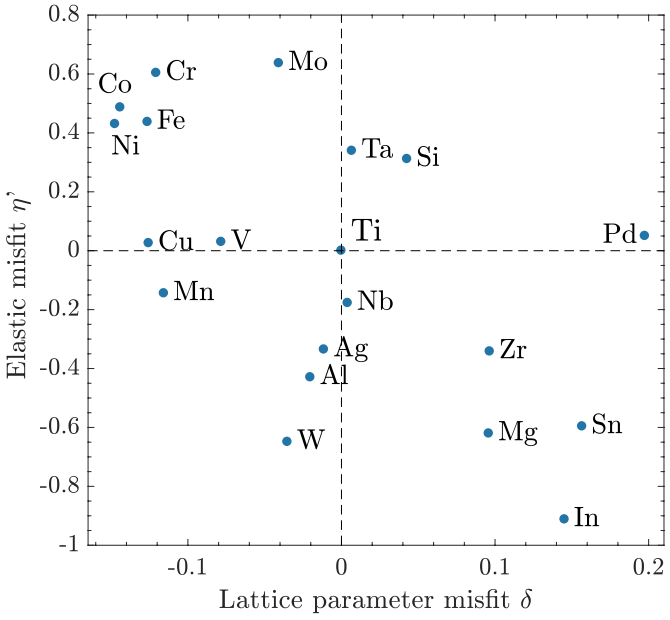

Fig. 2. Lattice parameter misfit δ and elastic modulus misfit η' between the 19 main alloying elements and the Ti solvent. Eutectoid β-stabilizers tend to show higher degree of misfit than that of isomorphous β-stabilizers.

Table 1
Shear moduli μ and Seitz radius R of major solutes in Ti alloys. Their misfit parameter λ and the SSH strengthening coefficient B_i are calculated accordingly.

Element	μ (GPa)	R (Å)	λ	B_i (MPa·at.$^{-2/3}$)
Ti	45.6	1.615	–	–
Pd	48	1.935	12.65	3023
Sn	18.4	1.869	10.31	2303
In	4	1.850	9.99	2207
Ni	80	1.377	9.59	2090
Co	88.8	1.383	9.42	2041
Fe	81	1.411	8.26	1715
Cr	115	1.421	8.09	1665
Cu	46.8	1.413	8.03	1650
Mn	39	1.429	7.42	1485
Mg	17.3	1.770	6.62	1276
Zr	30	1.771	6.33	1201
V	46.7	1.489	5.01	879
Mo	125.5	1.550	3.64	575
W	160	1.559	3.64	574
Si	66.2	1.684	3.01	445
Al	26	1.583	2.15	285
Ag	30.3	1.597	1.53	181
Ta	69	1.626	1.42	164
Nb	37.5	1.622	0.76	71

The measured microstrain and dislocation density by Rietveld refinement are listed in Table 2. The alloys showed a large dislocation density, which is induced by a strong lattice distortion during rapid solidification. SSH also makes a considerable contribution in the range of 477–561 MPa with increasing Fe content. The rest of the contribution comes from the Hall-Petch effect (less than 300 MPa). The Hall-Petch constant of each alloy is respectively 0.94, 0.97 and 1.00 MPa·m$^{1/2}$ with Fe content increasing.

The strain hardening of the Ti-Fe-Sn-Nb alloys in plastic deformation are mainly promoted by dislocation storage and dislocation interactions. Fig. 3 illustrates the experimental stress-strain curves in compression and the modelled flow stress evolution. The deformation condition is under a constant strain rate $\dot{\varepsilon} = 1.0\times10^{-4}s^{-1}$ at room temperature. The initial dislocation density ρ_0 of each alloy applies the data in Table 2. The model shows good agreement with the experimental data when the dislocation storage coefficient $k = 0.12$ and the annihilation coefficient $f = 3.6$, suggesting the macroscopic mechanical response can be well described. The parameters and their values involved in the calculation are listed in Table 3.

The yield stress prediction by Eq. (7) was applied to Ti-Mo-Fe, Ti-Mo-Zr-Fe, Ti-Mo-Zr-Al, Ti-Mo-Fe-Al, Ti-V-Al, Ti-V-Cr-Mo-Zr-Al, Ti-V-Cr-Al-Sn, Ti-V-Mo-Fe-Al and Ti-Fe-Nb systems [15,23–25] as shown in Fig. 4. The error bars in the calculated yield stresses result from the approximation of the stored strain energy in the alloys that are subjected to different manufacturing conditions and thermomechanical

Table 2
The microstrain ε_{micro}, average dislocation density ρ_0, as well as the evaluations of forest hardening σ_ρ, solid solution hardening σ_{ss}, grain boundary strengthening σ_{HP} and the calculated yield stress σ_Y. The stress unit is MPa.

Alloy (wt.%)	$\varepsilon_{micro}\times10^{-3}$	$\rho_0\times10^{15}$	σ_ρ	σ_{ss}	σ_{HP}	σ_Y
Ti-11Fe-7Sn-5Nb	4.639	1.815	408	477	271	1337
Ti-13Fe-7Sn-5Nb	4.886	2.014	430	520	281	1410
Ti-15Fe-7Sn-5Nb	5.197	2.278	457	561	290	1486

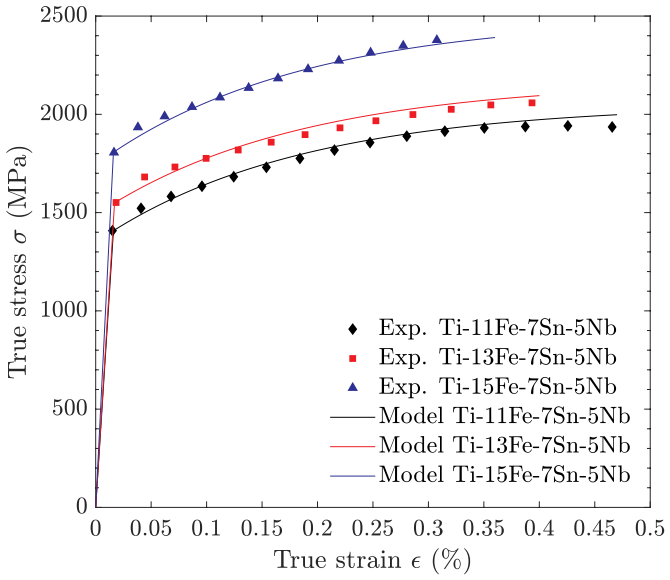

Fig. 3. Experimental true stress-strain curves and the modelled evolution of the flow stress as a function of strain. The initial dislocation density in the model applies the result approximated by the stored elastic energy (Table 2). The strain hardening mainly generated by the accumulation of dislocations in compression.

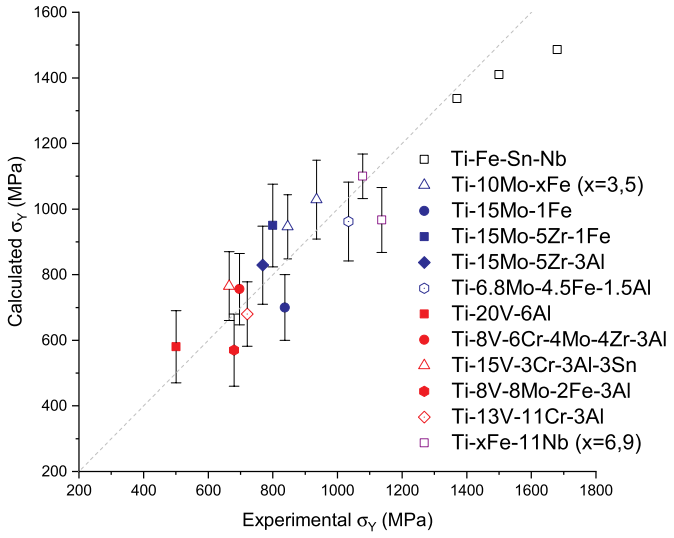

Fig. 4. Experimental *vs.* calculated yield stress. The alloys with the same main alloying element (e.g. Mo, V, or Fe) were identified by colour. The reference β-type alloys were collected from literature [15,23–25] with dislocation slip dominating the deformation mode. All compositions are given in wt.%. (For interpretation of the references to colour in this figure legend, the reader is referred to the Web version of this article.)

Table 3
Physical parameters and mechanical features of the Ti alloys involved in calculations.

Parameter	Physical description	Value	Ref.
M	Taylor factor	2.8	[7]
E	Elastic modulus	102 GPa	[17]
μ	Shear modulus	39 GPa	[16]
ν	Poisson's ratio	0.32	[16]
θ	Interaction parameter between screw and edge dislocations	16	[4]
Z	Temperature-dependent numerical factor	0.9×10^{-3}	[4]
k_{Ti}	Hall-Petch constant of pure Ti	0.75 MPa·m$^{1/2}$	[9]
α	Dislocation interaction constant	0.3	[12]
D	Mean grain size	12 μm	[16]
b	Magnitude of Burgers vector	2. 8 Å	[16]
k	Dislocation storage coefficient	0.12	fitted
f	Dislocation annihilation coefficient	3.6	fitted

treatments. For alloys prepared by injection or suction casting, the dislocation density is in the range of $\sim 10^{15}$ m^{-2}, while the solution treated alloys kept the dislocation density approximately in the order of 7.5×10^{13} to 1×10^{14} m^{-2} [26,27].

Systems with a eutectoid β-stabilizer as main alloying element tend to provide more SSH. Besides, it is interesting to note that the SSH can be further improved by adding a minor amount of the neutral element Sn due to its high strengthening coefficient B_i. However, it should be born in mind that over 5 at.% Sn may lead to the formation of the intermetallic Ti_3Sn phase [28]. The processing parameters and the thermomechanical treatments not only affect the grain size, but also influence the stored strain energy. The yield stress and the strain hardening models were built via a dislocation-glide-based approach. On the other hand, the yield stress deduction induced by mechanical twinning or phase transformation would be the next natural step for future work.

5. Conclusions

In summary, the strengthening model can be used to quantify the effect of each solute element, as well as to appraise the contribution of each strengthening mechanism. A generalised expression for the yield stress was derived by integrating the strengthening from solid solution, grain boundary and dislocation forest. Eutectoid β-stabilisers e.g. Cr, Co, Ni, Fe and Cu exhibit great SSH coefficient due to the more pronounced shear modulus and lattice parameter misfits. Besides, dislocation forest strengthens the alloys significantly owing to the heavy lattice distortion and large dislocation density, especially for alloys produced by rapid solidifications. The strain-hardening in plastic deformation of the Ti-Fe-Sn-Nb alloys is mainly induced by dislocation interactions, which feature was well described by competitions between dislocation storage and annihilation terms. Furthermore, the model can be applied to optimise and design Ti alloys to improve their combined strength and plasticity.

Acknowledgements

This work is supported by Designing Alloys for Resource Efficiency (DARE) EP/L025213/1 from the UK Engineering and Physical Science Research Council (EPSRC).

References

[1] E.I. Galindo-Nava, P.E.J. Rivera-Díaz-del-Castillo, Acta Mater. 128 (2017) 120–134.
[2] P. Castany, M. Besse, T. Gloriant, Scripta Mater. 66 (2012) 371–373.
[3] R. Labusch, Phys. Status Solidi 41 (1970) 659–669.
[4] L. Čižek, P. Kratochvíl, B. Smola, J. Mater. Sci. 9 (1974) 1517–1520.
[5] L. Gypen, A. Deruyttere, J. Mater. Sci. 12 (1977) 1028–1033.
[6] I. Toda-Caraballo, P.E.J. Rivera-Díaz-del-Castillo, Acta Mater. 85 (2015) 14–23.
[7] J. Rosenberg, H. Piehler, Metall. Trans. 2 (1971) 257–259.
[8] I. Toda-Caraballo, E.I. Galindo-Nava, P.E.J. Rivera-Díaz-del-Castillo, Acta Mater. 75 (2014) 287–296.
[9] D. Wu, J. Zhang, J. Huang, H. Bei, T.-G. Nieh, Scripta Mater. 68 (2013) 118–121.
[10] R. Madec, B. Devincre, L. Kubin, Phys. Rev. Lett. 89 (2002) 255508.
[11] A. Argon, Strengthening Mechanisms in Crystal Plasticity vol. 4, Oxford University Press on Demand, 2008.
[12] L. Kubin, B. Devincre, T. Hoc, Mater. Sci. Eng. A 483 (2008) 19–24.
[13] U. Kocks, H. Mecking, Prog. Mater. Sci. 48 (2003) 171–273.
[14] B. Devincre, T. Hoc, L. Kubin, Science 320 (2008) 1745–1748.
[15] P.J. Bania, JOM 46 (1994) 16–19.
[16] G.-H. Zhao, High-performance Load-Bearing Alloys, Ph.D. thesis KTH Royal Institute of Technology, 2017.
[17] G.-H. Zhao, S.V. Ketov, J. Jiang, H. Mao, A. Borgenstam, D.V. Louzguine-Luzgin,

Mater. Sci. Eng. A 705 (2017) 348–351.
[18] A. Borbély, J. Driver, T. Ungár, Acta Mater. 48 (2000) 2005–2016.
[19] B. Kim, E. Boucard, T. Sourmail, D. San Martín, N. Gey, P.E.J. Rivera-Díaz-del-Castillo, Acta Mater. 68 (2014) 169–178.
[20] F. Christien, M. Telling, K. Knight, Scripta Mater. 68 (2013) 506–509.
[21] V. Lubarda, Mech. Mater. 35 (2003) 53–68.
[22] G.-H. Zhao, H. Mao, D.V. Louzguine-Luzgin, J. Appl. Phys. 120 (2016) 205106.
[23] S. Hanada, O. Izumi, Metall. Mater. Trans. 18 (1987) 265–271.
[24] K. Tsuzaki, S. Emura, T. Nishimura, K. Tsuchiya, Mater. Trans. 52 (2011) 1611–1616.
[25] S. Ehtemam-Haghighi, Y. Liu, G. Cao, L.-C. Zhang, Mater. Des. 97 (2016) 279–286.
[26] M. Ahmed, D.G. Savvakin, O.M. Ivasishin, E.V. Pereloma, Mater. Sci. Eng. A 576 (2013) 167–177.
[27] X. Ji, S. Emura, X. Min, K. Tsuchiya, Mater. Sci. Eng. A 707 (2017) 701–707.
[28] G.-H. Zhao, S.V. Ketov, H. Mao, A. Borgenstam, D.V. Louzguine-Luzgin, Scripta Mater. 135 (2017) 59–62.